X-ray Scattering Studies of Maquette Peptide Monolayers. 2. Interferometry at the Vapor/Solid Interface

Joseph Strzalka,*,† Xiaoxi Chen,‡ Christopher C. Moser,‡ P. Leslie Dutton,‡ John C. Bean,§ and J. Kent Blasie†

Department of Chemistry and Department of Biochemistry and Biophysics, University of Pennsylvania, Philadelphia, Pennsylvania 19104, and Department of Electrical Engineering, University of Virginia, Charlottesville, Virginia 22904

Received July 1, 2000. In Final Form: November 2, 2000

We apply X-ray interferometry to study the profile structure of Langmuir−Blodgett (LB) monolayers containing maquette peptides, *de novo* di-α-helical synthetic peptides designed as model systems for studying biological electron transfer. The results demonstrate that it is possible to create monolayers with the peptide vectorially oriented with its helical axis (the direction of electron transfer within the holopeptide) approximately normal to the surface of the solid support. This orientation can even be achieved when the orientation of the peptide in the precursor Langmuir film at the air/water interface is parallel to the surface, indicating that reorganization of the monolayer can occur during or after LB deposition. Though issues regarding the low density of the film and variability between samples remain to be addressed, the work represents an important step toward future correlated functional/structural studies of these peptides.

Introduction

Maquette peptides form the basis of an approach to understanding the behavior of redox protein complexes, which perform an array of vital functions including respiration and photosynthesis. Redox protein complexes are typically large and membrane-bound and, hence, difficult to purify and study. In contrast, synthetic maquette peptides are smaller, simpler, soluble peptides designed to mimic a part of the structure and function of natural redox complexes. We seek to understand proteins better by constructing our own. Inspired by part of the transmembrane domain of cytochrome bc_1, the four-helix bundle motif comprises the basic structural design of one family of maquettes.[1] In the prototype, a 31-mer peptide is synthesized, designed as 27 residues forming an amphipathic α-helix and the other residues a short, flexible loop ending in a cysteine residue at the N-terminus of the peptide. In solution, a disulfide bond forms between the cysteines of two helices, forming a dihelical unit. The hydrophobic effect apposes the two helices, forming a pair of bis-His binding sites for prosthetic groups between the helices, and further drives the association of dihelical units into four-helix bundles.

Structural and functional characterization of the peptides plays a central role in the maquette peptide program. It is important to compare the product synthesized with the intended design and to compare its functions with those of natural proteins. For the electron transfer properties of proteins, these two aspects of characterization are coupled, as the determination of a rate of electron transfer must be accompanied by knowledge of the distance and medium through which it occurs to be most meaningful. X-ray interferometry on oriented monolayers can provide the profile structure, the average structure of the monolayer projected onto the coordinate normal to its surface, and also preserve the peptide in an environment in which its function can also be studied. For the most thorough characterization, the peptide should ideally be oriented so that the direction of electron-transfer coincides with the normal to the monolayer surface, the direction probed by interferometry. Part 1 of this study demonstrated that the orientation of maquette peptides in a monolayer at the air/water interface can be controlled via the macroscopic parameter π, the surface pressure of the film.[2] Although the order of Langmuir films is not always maintained upon transfer to a solid support,[3−5] the finding suggests that Langmuir−Blodgett (LB) deposition of maquette peptide films may produce a suitably ordered film.

In this study, we spread monolayers of two different maquette peptides, the original prototype and a variant with a C_{16} saturated hydrocarbon chain coupled to the free amine group of the N-terminal cysteine of each α-helix. Using Langmuir−Blodgett techniques, we transfer the monolayers from the air/water interface to solid supports incorporating an inorganic reference structure, and investigate the profile structure of these films using X-ray interferometry. In an important step toward future correlated structural/functional studies, we demonstrate that in each system the peptide does orient within the monolayer with the long axis of the helices, presumably the direction of electron transfer between the prosthetic group binding sites, aligned approximately along the normal to the surface of the support. Differences between the expected and observed profile structures and implications for future work are also discussed.

* To whom correspondence may be addressed: Department of Chemistry, Box 141, University of Pennsylvania, Philadelphia, PA 19104-6323; e-mail, strzalka@jkb2.chem.upenn.edu.

† Department of Chemistry, University of Pennsylvania.

‡ Department of Biochemistry and Biophysics, University of Pennsylvania.

§ Department of Electrical Engineering, University of Virginia.

(1) Robertson, D. E.; Farid, R. S.; Moser, C. C.; Urbauer, J. L.; Mulholland, S. E.; Pidikiti, R.; Lear, J. D.; Wand, A. J.; DeGrado, W. D.; Dutton, P. L. *Nature* **1994**, *368*, 425−431.

(2) Strzalka, J.; Chen, X.; Moser, C. C.; Dutton, P. L.; Bean, J.; Blasie, J. K. *Langmuir* **2000**, *16*, 10404.

(3) Hann, R. A. Molecular Structure and Monolayer Properties. In *Langmuir−Blodgett FIlms*; Robserts, G., Ed.; Plenum Press: New York, 1990.

(4) Riegler, J. E.; LeGrange, J. D. *Phys. Rev. Lett.* **1988**, *21*, 2492−2495.

(5) LeGrange, J. D. *Phys. Rev. Lett.* **1991**, *66*, 37−40.

10.1021/la0009285 CCC: $20.00
Published on Web 01/26/2001

Methods and Materials

We used the same peptides as in our investigation of maquette peptide Langmuir films, namely, the prototypical four-helix bundle denoted H10H24[1]

CGGGE LWKLH EELLK KFEEL LKLHE ERLKK L
1

and a palmitoylated peptide denoted BBC16, which is the same except for amino acid substitutions at positions 6 and 13[6,7]

$CH_3(CH_2)_{14}CO-$CGGGE IWKLH EEFLK KFEEL
1
LKLHE ERLKK L

Both were synthesized via solid phase methods on a commercially available machine.[8] Spreading solutions were typically 100 μM in 50 mM TRIS buffer with 100 mM NaCl. We used *apo* BBC16 and *hemo* H10H24, with a stoichiometric amount of Fe-protoporphyrin IX[9] titrated in from a concentrated DMSO stock solution.

We spread the peptide monolayers onto the meniscus of a glass capillary obliquely penetrating the air/water interface of a 1 mM TRIS subphase at pH 8, 23 °C, contained in a commercial Langmuir trough with a dipping head (Lauda). For the 4:1 palmitic acid/BBC16 mixed monolayer, the subphase also contained 1 mM $CdCl_2$, and the lipid was spread from a 1 mM chloroform solution directly onto the interface with a 3-min pause before the peptide was spread. After waiting 20 min, we compress the monolayer at 1−2 Å^2/(α-helix/s) and then maintained constant pressure, π_{dep}, during LB deposition. For H10H24 samples, π_{dep} = 20 or 25 mN/m and the slides were plunged through the interface quickly and withdrawn slowly (2 mm/min) with transfer occurring on the upstroke only. For samples containing BBC16, π_{dep} = 45 mN/m, we deposit on the downstroke at a rate of 3 mm/min and aspirate the monolayer before withdrawing the sample from the subphase.

LB film samples were refrigerated in vials with a reservoir of KNO_3 in order to maintain relative humidity at 96%. During data collection (12−16 h), samples were maintained at 4 °C and in humidity in excess of 90% using a humidity generator.[10]

The solid supports used for LB deposition were 2 × 1 cm^2 slides cleaved from a 4-in. Si wafer with a superlattice structure deposited onto its surface by molecular beam epitaxy (MBE).[11] The superlattice contains three unit cells of 2 Ge and 30 Si atomic layers: $3(Ge_2Si_{30})$. As the MBE deposition occurs under ultrahigh vacuum conditions and the wafers are stored in an inert atmosphere, we did not need to clean the wafers other than by sonication in various solvents (10 min each in methanol, chloroform, and acetone). We characterized them by collecting 2 h of meridional X-ray diffraction data for each slide in a dry helium environment at room temperature.

After characterization, we deposited self-assembled monolayers (SAMs) onto the MBE slides. For H10H24 samples, we fabricated mercaptopropylsilane (MPS) SAMs[12] according to the procedure of a study that demonstrated a favorable interaction between MPS SAMs and H10H24 in solution.[13] For samples containing BBC16, we used SAMs of a saturated C_{18} hydrocarbon chain from the precursor octadecyltrichlorosilane (OTS). The procedure, based on that of Sagiv,[14] has been used commonly in our group to prepare surfaces for LB deposition of fatty acid films.[15−17] Immediately following chemisorption of the SAMs, we characterized them by collecting about 12 h of X-ray interferometry data in a dry environment at room temperature.

The setup for meridional X-ray diffraction has been described in detail in the past.[18] We use a line focused beam 6 mm high from a rotating anode source monochromated to select the Cu Kα wavelength λ = 1.54 Å. Slits upstream of the sample define the incident beam, but there are no slits before the 2-D position-sensitive proportional counter that we use as the detector. This allows us to keep the detector fixed and integrate the total intensity as we oscillate the sample through a range of incident angles ω in the beam and collect a range of interferometry data from ω_{min} to ω_{max}. This corresponds to a range of momentum transfer perpendicular to the surface of the sample, $q_z \equiv (2/\lambda) \sin \omega$. Note that we adopt our usual convention and not the one used in part 1 of this study in which the definition was larger by a factor of 2π, as customary in reflectivity studies.

We apply box refinement, a model-independent, iterative procedure, to obtain the electron density distribution $\rho(z)$ that reproduces the experimentally observed diffraction intensity function, $I_{exp}(q_z)$.[19,20] The method can be applied under two conditions: (1) the structure must be finite in extent; (2) the amplitude of the diffraction intensity and the structure must be Fourier transform pairs. The first condition will be met for the profile structure of any sufficiently thin film. The second condition, equivalent to the first Born approximation, means that the method can only be applied to the kinematical diffraction from a sample, that is, the photons in the scattered beam that have undergone only a single scattering event, and not the more intense dynamical diffraction, which includes multiple scattering, that begins to dominate, progressively, the specular reflectivity as one approaches the critical angle for total external reflection from the sample.[21] Recent treatments of the theory underlying synchrotron-radiation-based reflectivity measurements demonstrate that the rigorously correct separation of these two components comes from normalizing the data by dividing out the Fresnel function, the mathematical description of the reflectivity from an abrupt interface between two different media.[22] In this formalism, the amplitude of the normalized reflectivity and the *derivative* of the profile structure, dρ/dz, constitute a Fourier transform pair. Our recent studies of lipid/peptide monolayers at the air/water interface applied box refinement to normalized reflectivity data in order to obtain dρ/dz, which could then be integrated to yield $\rho(z)$.[2,23] In this study, because the area detector integrates both the dynamical/kinematical diffraction and the background scattering (from the dry or humid helium and components of the flight path) occurring during the oscillation of the sample, we return to a pragmatic approach of extracting the kinematical diffraction from the data, an approach used successfully within our lab in earlier studies of thin films on solid substrates.[15,24,25] The method, illustrated in Figure 1 for several datasets, consists of approximating the underlying dynamical diffraction and background scattering as a piecewise continuous sum of exponentials, which approximates the data collected from a uniform silicon substrate using our setup. The details of the correction appled here will not affect the positions of features in the data, the most important determinants of the structure.

(6) Gibney, B. R.; Rabanal, F.; Skalicky, J. J.; Wand, A. J.; Dutton, P. L. *J. Am. Chem. Soc.* **1997**, *119*, 2323−2324.
(7) Skalicky, J. J.; Bieber, R. J.; Gibney, B. R.; Rabanal, F.; Dutton, P. L.; Wand, A. J. *J. Biol. NMR* **1998**, *11*, 227−228.
(8) Chen, X.; Moser, C. M.; Pilloud, D. L.; Dutton, P. L. *J. Phys. Chem. B* **1998**, *102*, 6425−6432.
(9) For the structure of Fe-protoporphyrin IX, see: Stryer, L. *Biochemistry*, 4th ed.; W. H. Freeman and Co.: New York, 1995; p 148.
(10) Gruner, S. M. *Rev. Sci. Instrum.* **1981**, *52*, 134−136.
(11) Hull, R., Bean, J. C., Eds. Germanium Silicon: Physics and Materials. *Semiconductors and Semimetals*; Academic Press: New York, 1999; Vol. 56.
(12) Goss, C. A.; Charych, D. H.; Majda, M. *Anal. Chem.* **1991**, *63* 85−88.
(13) Pilloud, D. L.; Rabanal, F.; Gibney, B. R.; Farid, R. S.; Dutton, P. L.; Moser, C. C. *J. Phys. Chem. B* **1998**, *102*, 1926−1937.
(14) Sagiv, J. *J. Am. Chem. Soc.* **1980**, *102*, 92−98.
(15) Skita, V.; Filipkowski, M.; Garito, A. F.; Blasie, J. K. *Phys. Rev. B* **1986**, *34*, 5826−5837.
(16) Fischetti, R. F.; Filipkowski, M.; Garito, A. F.; Blasie, J. K. *Phys. Rev. B* **1988**, *37*, 4714−4726.
(17) Richardson, W.; Blasie, J. K. *Phys. Rev. B* **1989**, *39*, 12165−12181.
(18) Edwards, A. M.; Chupa, J. A.; Strongin, R. M.; Smith, A. B., III; Blasie, J. K.; Bean, J. C. *Langmuir* **1997**, *13*, 1634−1643.
(19) Stroud, R. M.; Agard, D. A. *Biophys. J.* **1979**, *25*, 495−512.
(20) Makowski, L. *J. Appl. Crystallogr.* **1981**, *14*, 160−168.
(21) Cowley, J. M. *Diffraction Physics*, 4th ed.; Elsevier Science Publishers: Amsterdam, 1990.
(22) Als-Nielsen, J.; Jacquemain, D.; Kjaer, K.; Leveiller, F.; Lahav, M.; Leiserowitz, L. *Phys. Rep.* **1994**, *246*, 251−313.
(23) Zheng, S.; Strzalka, J.; Ma, C.; Opella, S. J.; Ocko, B. M.; Blasie, J. K. *Biophys. J.*, in press.
(24) Xu, S.; Fischetti, R. F.; Blasie, J. K.; Peticolas, L. J.; Bean, J. C. *J. Phys. Chem.* **1993**, *97*, 1961−1969.
(25) Murphy, M. A.; Blasie, J. K.; Peticolas, L. J.; Bean, J. C. *Langmuir* **1993**, *9*, 1134−1141.

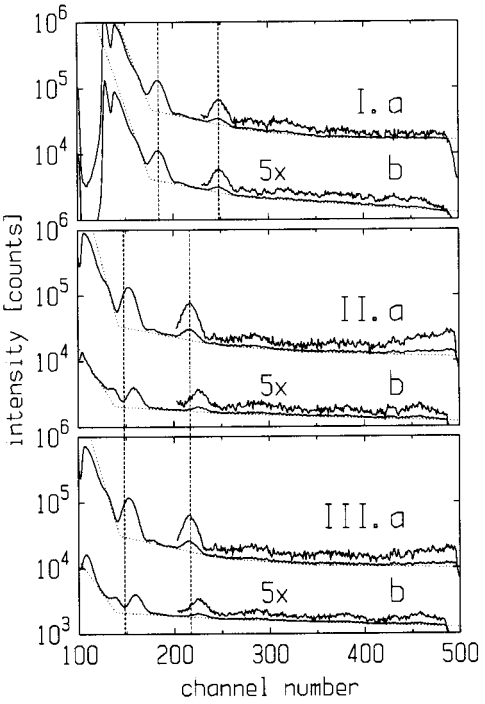

Figure 1. Strip-integrated experimental intensity data after uniformity correction, with the dynamical diffraction and background scattering indicated (dotted). Panel I. (a) Bare substrate incorporating an MBE reference structure. (b) Same sample after deposition of an MPS SAM—the diffraction is unchanged because the maximum length of MPS is comparable to the experimental resolution. Panels II and III. (a) Bare substrate incorporating an MBE reference structure. (b) Same sample after deposition of an MPS SAM and LB deposition of a monolayer of pure H10H24. Dashed vertical lines are intended to guide the eye toward similarities and differences between patterns. The overall shift to the right between panels I and II is due to repositioning of the detector between experiments and is accounted for in the analysis. Data were analyzed out to the minimum in the vicinity of channel 350.

Recently in the preparation of one study, both approaches were applied to data collected from a yeast cytochrome *c* monolayer on a nonpolar SAM and were shown to yield similar results.[26]

Using our pragmatic approach, we consider the dynamical and kinematical diffraction as arising from different Fourier components of the sample's profile structure. The dynamical diffraction arises from the mean electron density of the sample, $\bar{\rho}(z)$, the components of the profile structure included in the range $q_z = 0$ to $q_z = q_{min}$, where q_{min} is the minimum q_z value contained in the background-corrected data. Meanwhile, the kinematical diffraction arises from the relative electron density (also called the electron density contrast), $\Delta\rho(z)$, the components of the profile structure in the range $q_z > q_{min}$, though this range is truncated at q_{max}, the point at which the reflectivity signal becomes weak and is no longer analyzed. The result that we obtain from box refinement will therefore be the experimentally determined relative electron density of the sample, $\Delta\rho_{exp}(z)$. For details of the application of the highly constrained box refinement algorithm to interferometry data, the reader is referred to the Analysis section of Xu et al.[24] As an aid in interpreting the box refinement results, we refine model profile structures on an absolute scale, $\rho_{mod}(z)$, whose relative electron densities, $\Delta\rho_{mod}(z)$, computed for the same range of q_z contained in $I_{exp,c}(z)$, match $\Delta\rho_{exp}(z)$ as closely as possible.

H10H24 Monolayers Deposited onto MPS SAMs

We characterized LB films of H10H24 deposited onto MPS-coated MBE supports on the upstroke at a surface pressures of 20 or 25 mN/m. At these pressures just before the plateau in the isotherm of the monolayer, the highest pressures that we could easily achieve and maintain during deposition, the H10H24 dihelix lies in the plane of the air/water interface.[2] MPS was previously found to interact well with H10H24 in solution and promote the formation of SAMs of the peptide.[13] Figure 1 shows the data collected from the H10H24 samples prepared for this study. The top panel (I) shows the data from the support before and after deposition of an MPS SAM. The bare support diffracts well, with three diffraction maxima visible (centered approximately at channels 180, 250, and 320; the features to the left are the scatter around the beamstop and the truncation of the specular reflectivity at the smallest incident angle included in the oscillation). The MPS SAM did not change the diffraction data from the bare sample, and so we did not collect it for subsequent samples. However, deposition of the LB monolayers produces marked destructive interference and changes the diffraction pattern, as seen in panels II and III. As compared to the data from the bare, the first maximum is split in the LB film data while the second maximum shifts to higher q_z. These effects can be clearly seen in the raw data and are not artifacts of the particular background subtracted here. As demonstrated in the Supporting Information, the autocorrelation function computed from the background-subtracted data indicates that the LB layer increases the size of the structure from about 130 Å to about 200 Å.

Inspection of the relative electron density profile structures obtained via box refinement reveals the features of the sample (Figure 2.b). In $\Delta\rho_{MBE}(z)$, the three largest peaks correspond to the Ge layers of the MBE superlattice. The doubly peaked feature corresponding to the surface of the support ends approximately at $z = 0$ due to our choice of the trial structure. The splitting of this feature has been seen before and indicates the presence of another interface near the support/air interface. As in the past, we attribute it to a low-density oxide layer, SiO_x, on top of the underlying Si.[24] The small features in $\Delta\rho_{MBE}(z)$ outside of -120 Å $< z <$ 0 Å are due to the truncation of the data at q_{min} and q_{max} and are not significant as they do not correspond to features in the Patterson function (Figure 2a). As the corrected data for the bare and MPS-coated support are virtually identical, so are $\Delta\rho_{MBE}(z)$ and $\Delta\rho_{SAM}(z)$. With our experimental resolution of $1/q_{max} = 1/0.09$ Å$^{-1} = 11$ Å, we are unable to detect the presence of the MPS monolayer. In contrast, the LB monolayer of H10H24 results in a markedly different profile structure, $\Delta\rho_{LB}(z)$. Here, the feature corresponding to the surface of the MBE support is still present, but diminished in amplitude, indicating that the change in density that occurs there has become smaller. New features appear in the region 0 Å $> z >$ 61 Å, making the total length of the profile structure about 180 Å long. Similar features occur in the relative electron density profiles obtained by the same methods for the other samples (see Supporting Information). In all cases, we see two maxima with some splitting in the approximate range 0 Å $> z >$ 60 Å (Table 1 summarizes the details). The model absolute electron densities, $\rho_{mod}(z)$, that account for the $\Delta\rho_{exp}(z)$ functions obtained from box refinement (Figure 2e) result in a peptide monolayer of fairly constant density about 25% that of bulk Si. The shape agrees with our expectations, but the density seems lower than we expected, as will be discussed below.

(26) Kneller, L. R.; Edwards, A. M.; Nordgren, C. E.; Blasie, J. K.; Berk, N. F.; Krueger, S.; Majkrzak, C. F. *Biophys. J.*, in press.

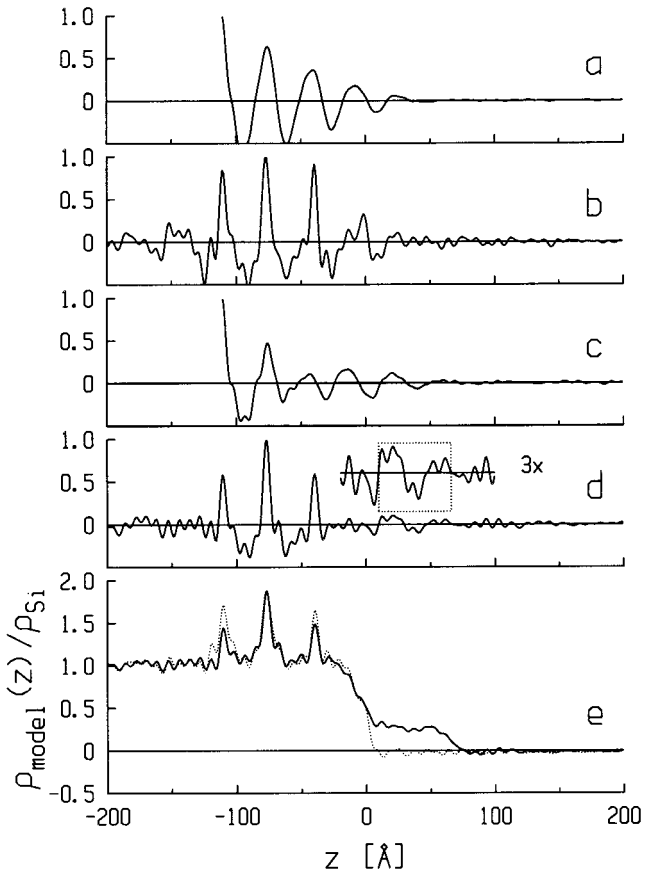

Figure 2. Steps in the analysis of the data collected from an H10H24 sample (Figure 1.II). (a) The generalized (half) Patterson function, or autocorrelation function of the bare MBE solid support, with its origin shifted to coincide with the innermost Ge peak in the relative electron density profile, $\Delta\rho_{exp}^{MBE}(z)$ (b). As indicated by the Patterson function, the last significant feature in $\Delta\rho_{exp}^{MBE}(z)$ occurs at the surface, $z = 0$ Å (see Supporting Information, Figure A1), which is perhaps more clear in the model absolute electron density profile structure $\rho_{mod}^{MBE}(z)$ (e, dotted curve) constructed to be consistent with $\Delta\rho_{exp}^{MBE}(z)$. (c) The generalized Patterson function for the MBE support with MPS SAM and H10H24 LB monolayer deposited shows that now the structure extends to about $z =$ 65 Å due to the presence of the peptide monolayer (boxed region in $\Delta\rho_{exp}^{LB}(z)$, inset of (d), and low-density region of $\rho_{mod}^{LB}(z)$ (e, solid curve).

Table 1. The Length of the Peptide in Various LB Monolayer Samples As Determined from the Relative Electron Density Profile Structures, $\Delta\rho_{exp}(z)$[a]

peptide	length (Å)	peptide	length (Å)
H10H24 model	44	BB NMR data	53
H10H24	65	BBC16	58
H10H24	65	4:1 PA/BBC16	66
H10H24	55	4:1 PA/BBC16	82[b]

[a] The lengths shown are the lengths of the dotted boxes indicating the peptide region of $\Delta\rho_{exp}(z)$ in the figures in this paper. When more than one value is given, the subsequent values come from profile structures of different samples shown in the Supporting Information. For comparison, the lengths of the longest projections from atomic coordinates (Figure 7b,b′) are also given. [b] Inspection of the $\rho(z)$ model that refined to agree with this $\Delta\rho(z)$ shows that the peptide region is only 69 Å long if the low-density region at the peptide/vapor interface is excluded.

BBC16 Monolayers Deposited onto OTS SAMs

The palmitoyl chains covalently bonded to the N-terminal cysteine of each α-helix of the peptide BBC16 help stabilize Langmuir monolayers of this peptide at high surface pressures. We prepared two different kinds of samples: pure BBC16 monolayers and mixed monolayers with free palmitic acid (PA) and BBC16 in a 4:1 ratio (4 mol of PA for each mole of single α-helices). We deposited LB monolayers at 45 mN/m on the downstroke onto MBE supports coated with OTS SAMs. At this pressure, the dihelices of BBC16 are approximately normal to the plane of the air/water interface.[2] This method relies on the van der Waals interaction between the C_{18} chains of the SAM and the C_{16} chains of the peptide to promote the deposition.

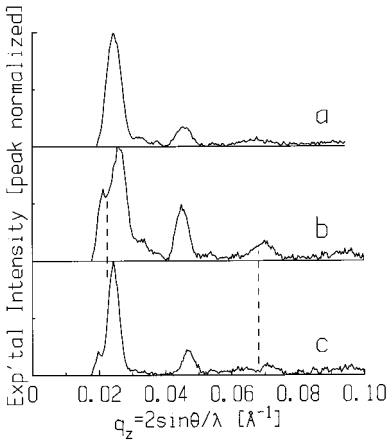

Figure 3. Corrected experimental X-ray intensity data for the experiment with the pure BBC16 LB monolayer, showing the same sample at different stages: (a) the bare MBE support; (b) the support with an OTS SAM deposited; (c) the support with the OTS SAM and LB monolayer of pure BBC16 deposited. The dashed lines point out the differences between the placement of minima due to destructive interference in (b) and (c).

The long SAM precursor used in these experiments (the all trans length of OTS is 23.1 Å) becomes immediately apparent in the X-ray interferometry data, where it causes destructive interference with the first maximum in the diffraction signal from the inorganic reference structure (Figure 3). Deposition of the peptide LB monolayer changes the signal further. These changes manifest themselves in the generalized Patterson functions, which both grow in extent at each stage in the sample processing and take on similar features (Figure 4). The similarities between the Pattersons indicate that the samples are about the same after deposition of the OTS SAM. However, at the deposition of the different LB films, pure BBC16 in one case and the 4:1 PA/BBC16 mixture in the other case, the samples take on different structures, as evidenced by the different Patterson functions. P_{LB}^{mix} extends about 20 Å further than P_{LB}^{pure} (see Supporting Information).

The relative electron density profile structures obtained via box refinement from the corrected data for the bare MBE supports (Figures 5a and 6a) are similar to each other, and their features can be assigned just as they were for the H10H24 experiment. Adding the OTS SAM diminishes the amplitude of the surface features of the reference structure and introduces a new peak approximately 20 Å further out in z (Figures 5b and 6b). This new feature is in turn diminished in the profile structure once the peptide LB monolayer is deposited onto the SAM. In the case of the pure BBC16 monolayer (Figure 5c), immediately after the SAM feature, the edge of the profile structure, the range 35 Å < z < 91 Å, shows features similar to those found at the edge of the profile structure for the H10H24 sample discussed in the previous section (Figure 2d). These features must belong to the profile structure of the peptide itself. Similar features appear again in the profile structure of the sample with the 4:1

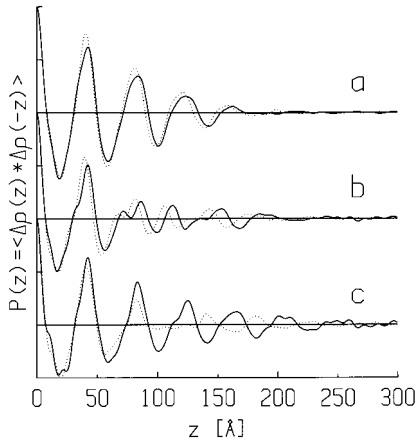

Figure 4. Generalized (half) Patterson functions for experiments with BBC16-containing monolayers, at different stages: (a) the bare MBE supports, $P_{MBE}^{pure}(z)$ (solid) and $P_{MBE}^{mix}(z)$ (dotted); (b) the support with an OTS SAM deposited, $P_{OTS}^{pure}(z)$ (solid) and $P_{OTS}^{mix}(z)$; (c) the support with the OTS SAM and LB monolayer containing BBC16 deposited. Here the sample preparation differs: one sample has a pure BBC16 monolayer, $P_{LB}^{pure}(z)$ (solid), while the other has a 4:1 palmitic acid/BBC16 mixed monolayer, $P_{LB}^{mix}(z)$ (dotted).

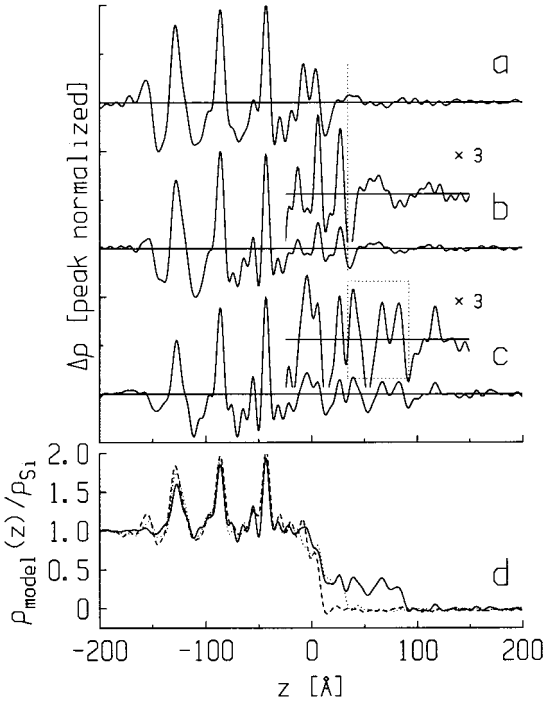

Figure 5. Relative electron density profile structures obtained via box refinement for the experiment with the pure BBC16 monolayer, at different stages: (a) The bare MBE support, $\Delta\rho_{MBE}^{pure}$. (b) The support with an OTS SAM deposited, $\Delta\rho_{OTS}^{pure}$. (c) The support with the OTS SAM and LB monolayer of pure BBC16 deposited, $\Delta\rho_{LB}^{pure}$. The insets show a 3-fold magnification of part of the structure directly beneath them. The dotted box in the inset of (c) contains the peptide and its left side, located at the SAM/LB film interface, extends upward to point out that $\Delta\rho_{OTS}^{pure}$ ends at about this position while $\Delta\rho_{MBE}^{pure}$ terminates earlier. (d) Model electron density profile structures on an absolute scale constructed to be consistent with the $\Delta\rho$ functions in (a) dashed, (b) dotted, and (c) solid curves.

PA/BBC16 monolayer, but they are displaced about 17 Å from the SAM feature by another peak, presumably due to the presence of the free palmitic acid in this sample (Figure 6c). The model $\rho(z)$ profiles constructed and refined as described in order to help interpret the experimental

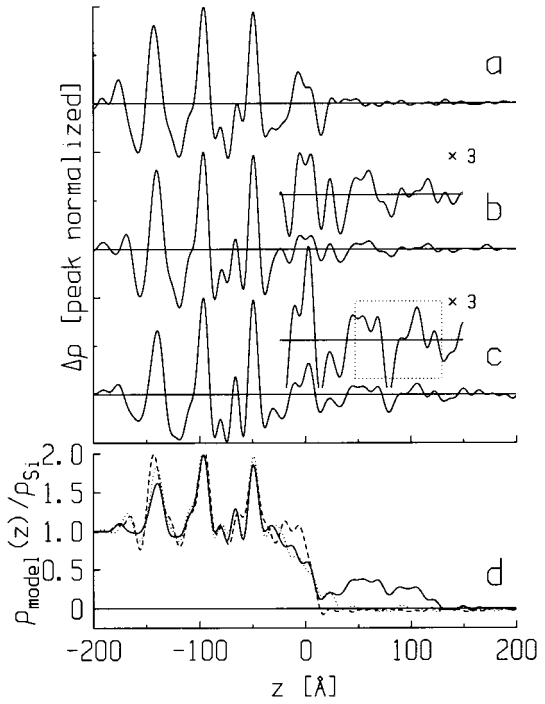

Figure 6. Relative electron density profile structures obtained via box refinement for the experiment with the 4:1 palmitic acid/BBC16 mixed LB monolayer, at different stages: (a) The bare MBE support, $\Delta\rho_{MBE}^{mix}(z)$. (b) The support with an OTS SAM deposited, $\Delta\rho_{OTS}^{mix}(z)$. (c) The support with the OTS SAM and the mixed LB monolayer deposited, $\Delta\rho_{LB}^{mix}(z)$. The insets show a 3-fold magnification of part of the structure directly beneath them. The dotted box in the inset of (c) contains the peptide. (d) Model electron density profile structures on an absolute scale constructed to be consistent with the $\Delta\rho$ functions in (a) dashed, (b) dotted, and (c) solid curves.

$\Delta\rho(z)$ profiles show that the density of the peptide region is about 30% of the density of silicon (Figures 5d and 6d).

Discussion

Two sources of atomic coordinates provide a basis for comparison between expectations and the experimental results. The first is a set of *model* atomic coordinates for *hemo* H10H24 that were developed as an aid in the design of the prototype maquette peptide.[1] The second source is the family of structures obtained *experimentally* from solution NMR studies of *apo* BB, the unpalmitoylated precursor of BBC16.[27,28] Both of these sources derive from the isotropic solution environment and so will have limited applicability to measurements of maquette peptides at interfaces. We projected the electron density from these sets of atomic coordinates onto the principal axes of the peptide using a spatial resolution consistent with that of the experiment. The scale of each projection was set by dividing it by the area obtained from the products of the widths (determined at 10% of the maximum value) of the other two projections. This rectangular approximation will include voids that are filled with water when the monolayer is at the air/water interface, so though the densities of the projections appear low, they are consistent with the calculations in the first part of this study. The projections appear in Figure 7, juxtaposed with the absolute electron density profile structures constructed and refined to explain the experimental results from this study. From

(27) Skalicky, J. J.; Gibney, B. R.; Rabanal, F.; Urbauer, R. J. B.; Dutton, P. L.; Wand, A. J. *J. Am. Chem. Soc.* **1999**, *121*, 4941−4951.
(28) Gibney, B. R.; Rabanal, F.; Skalicky, J. J.; Wand, A. J.; Dutton, P. L. *J. Am. Chem. Soc.* **1999**, *121*, 4952−4960.

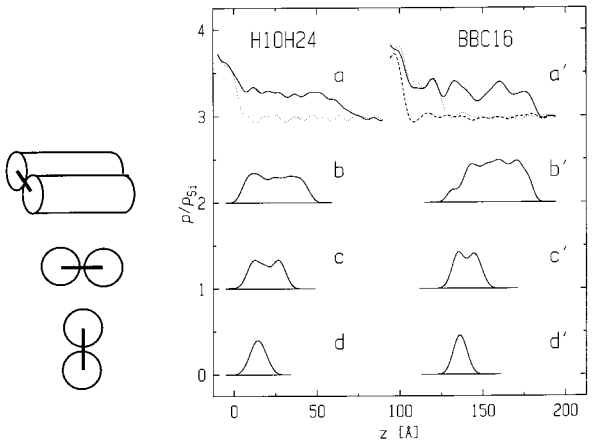

Figure 7. Comparison of the absolute electron density profile structures constructed and refined to agree with $\Delta\rho_{exp}(z)$, and projections computed from atomic coordinates: (a) H10H24 LB monolayer on an MPS SAM (solid line) on an underlying inorganic support (dotted); (b−d) projections computed from *model* atomic coordinates used in the design of H10H24;[1] (a′) pure BBC16 LB monolayer (solid line) on an OTS SAM (dotted) on an underlying inorganic support (dashed); (b′−d′) projections computed from the solution structure of BB, the unpalmitoylated precursor of BBC16, determined by NMR.[27,28] The schematics to the left of the diagram indicate the different projections onto the *z*-axis: (b, b′) with the helical axes parallel to the *z*-axis; (c, c′) with the helical axes perpendicular and the disulfide bond parallel to the *z*-axis; (d, d′) with the helical axis and the disulfide bond perpendicular to the *z*-axis.

inspection it is clear that the profiles we observe can only be consistent with the projection of the atomic coordinates onto the helical axis of the peptide.

At the same time, it is also clear that the profile structures of the LB monolayers are not identical with the projections. The H10H24 model coordinates predicted more supercoiling of the α-helices than was observed experimentally for the solution structure of BB, so that they probably underestimate the length of the peptide. In the profile structures determined for H10H24 monolayers, one sample agrees with the length predicted from the BB NMR structure while the other two cases exceed this length (see figure in Supporting Information and Table 1). The length of the pure BBC16 sample agrees well with that from the longest projection of the BB NMR solution structure, though the features within the profile vary. In particular, BB has a low density region in its projection at the N-terminus, where the Gly_3-Cys-Cys-Gly_3 flexible loop joins the two α-helices (left side of Figure 7b′), while the profile structure of BBC16 has a relatively high density there. As we do not see evidence of a distinct hydrocarbon chain region within the profile structure of BBC16, this enhanced density is probably due to the presence of folded hydrocarbon chains mingling with the flexible loop region of the peptide. Given the orientation of the peptide, we expect the chains to be highly disordered and collapsed (or folded) since these moieties have a minimal cross-sectional area of 20 Å^2 for fully extended chains, which is much smaller than that for α-helices (≥100 Å^2), and thus are constrained to exist at large excess area (at $\pi_{dep} = 45$ mN/m, about 115 Å^2).[2]

Judging from the absolute $\rho(z)$ models (Figure 6d), in the 4:1 PA/BBC16 mixture samples the peptide appears about 25 Å further away from the edge of the SiO_x layer, consistent with a denser, distinct hydrocarbon chain layer. It would seem, then, that the free fatty acid that we added to the monolayer occupies the excess area around each of the covalently bound palmitoyl chains, resulting in a well-packed hydrocarbon chain region. In our study of precursor 4:1 PA/BBC16 mixed Langmuir monolayers, the highest surface pressure that we studied was only 32 mN/m, when the area/α-helix is considerably larger, about 150 Å^2. As a result, we did not observe a well-defined hydrocarbon region in the profile structure of the precursor Langmuir film.[2]

The H10H24 monolayers also differ in structure from what we have seen in the precursor Langmuir monolayers, and this is more significant because the low surface pressure at which LB deposition occurred was included in our study. At low pressures below the plateau in the isotherm, the peptide exists as dihelices lying parallel to the air/water interface. But our results here show that in the LB film the peptide is oriented approximately normal to the air/solid interface, indicating a change in the monolayer structure that occurs during or after LB deposition. Changes in the optical properties of monolayers during LB deposition have been reported in other amphiphilic systems.[3−5] In this system, the reorientation may be promoted by the MPS SAM, which would present a fairly hydrophobic surface to the peptide if neighboring sulf-hydryl groups form disulfide bonds or if the SAM is sparse and highly tilted, as our inability to detect the SAM might suggest. The peptide may then prefer to remain in contact with the humid air rather than extend the surface area of its interaction with the SAM. A similar, though less pronounced, effect has been observed in molecular dynamics simulations of cytochrome *c* molecules on nonpolar versus polar surfaces.[29] This reorientation of the molecules may account for the lower density of the H10H24 samples compared to the BBC16 samples.

The average density of the H10H24 sample, 0.20 e$^-$/Å^3, or 28% the density of bulk Si, is about the same as that predicted by the projection from the model coordinates. The BBC16 sample is on average somewhat denser, 0.22 e$^-$/Å^3, with its peak density as high as 0.28 e$^-$/Å^3, though still not as dense as the solution structure predicts (0.32 e$^-$/Å^3, 45% of the density of Si). This density level, 0.32 e$^-$/Å^3, would also be expected for a well-ordered OTS SAM,[30] but the sample here has a mean density of only 0.28 e$^-$/Å^3, and a thickness of 18 Å, compared to the molecule's fully extended length of 24.3 Å. The OTS SAMs for the mixed BBC16 monolayers were less dense than that for the pure BBC16 sample. Overall, these somewhat lower densities must result from suboptimal packing of the constituent molecules of the film. Lateral inhomogeneities in the film would result in reflectivity that is a superposition of that from the bare support and that from the support plus film and cannot produce the destructive interference minima that we observed.

Since the projections were computed from atomic coordinates without water present, the conclusion is that there is very little water present in these films. One possible interpretation is that the peptide is denatured, since its hydration level keeps it out of the range of electron densities generally observed for proteins (0.40−0.45 e$^-$/Å^3).[31] However, the study was performed under conditions similar to those used in studies that demonstrated reasonable results for the profile structure of cytochrome *c*,[32] a protein of known structure and of a size roughly

(29) Nordgren, C. E.; Blasie, J. K. Manuscript in preparation.
(30) Tidswell, I. M.; Ocko, B. M.; Pershan, P. S.; Wasserman, S. R.; Whitesides, G. M.; Axe, J. D. *Phys. Rev. B* **1990**, *41*, 1111−1128.
(31) Perkins, S. J. X-ray and Neutron Solution Scattering. In *Modern Physical Methods in Biochemistry*; Neuberger, A., Van Deenen, L. L. M., Eds.; *New Comprehensive Biochemistry*; Elsevier: Amsterdam, 1988; Vol. 11B
(32) Amador, S. M.; Pachence, J. M.; Fischetti, R.; McCauley, J. P., Jr.; Smith,, A. B., III; Blasie, J. K. *Langmuir* **1993**, *9*, 812−817.

comparable to the BBC16 dihelix (104 vs 62 residues, respectively). Furthermore, the amount of water necessary to hydrate a protein monolayer remains an open question currently under investigation within our group. Molecular modeling calculations can show that a monolayer of water on cytochrome *c* molecules in a single monolayer requires only about 500 water molecules per cyt. *c*, only about 20% of the water necessary to fill the voids between protein molecules with bulk water.[29] A neutron scattering study of a cytochrome *c* monolayer at 88% relative humidity detected only 150−300 H2 O/cyt. *c*.[26] Then by analogy with cytochrome *c*, the BBC16 LB film might have 62/104 as many water molecules, or 90−180 H_2 O/dihelix, which would contribute about 0.06−0.12 $e^-/Å^3$ to the overall density of the film. (These numbers are somewhat lower than our estimate of the water content of the precursor langmuir film from part 1, 230 H_2O/dihelix at 40 mN/m.) As expected for an interferometric method, the modeling procedure used to put the profile structures on an absolute scale is very sensitive to the positions of interfaces ($\Delta z <$ 1 Å), but not so sensitive to the changes in electron density ($\Delta\rho \approx 0.06$ $e^-/Å^3$), so that a significant amount of water, enough to maintain the integrity of the peptide, may simply escape detection in our X-ray measurement. Ultimately, the water content of the film is best quantified by neutron measurements, while the state of the peptide can only be determined by correlated functional (spectroscopic or electrochemical) measurements.

Considering the variability among samples, it is clear that the optimal experimental design would determine the functional and structural parameters of the same sample. Rigorously applied protocols may improve the uniformity of the samples and permit this requirement to be relaxed so that it suffices to characterize representative samples structurally and other samples functionally via electrochemistry or spectroscopic methods. This would be important since the electrochemical measurements performed to date on self-assembled films use a gold electrode beneath a dimercaptoalkane SAM,[33] and the high electron density of gold makes it inconvenient for X-ray experiments. Similarly, the opaque MBE substrates used here are incompatible with the spectroscopic methods used to characterize the redox behavior of the peptides so far.[8,13]

However the orientation of the peptide molecules within the LB film comes about, producing films with the peptide's helical axis normal to the surface of the support advances the utility of maquette peptides as tools for model systems for studying biological electron transfer. In this orientation, the amino acid sequence of the peptide essentially maps simultaneously onto the direction that we are able to probe with reflectivity experiments and the direction of electron transfer in an electrochemical experiment. Using neutron interferometry and a series of (isomorphous) H^2-labeled peptides, we can in principle determine the location of any single amino acid within the profile structure of the peptide and so observe how binding prosthetic groups perturbs the structure of the peptide. (This technique would also be compatible with the incorporation of a gold electrode into the solid support.) Moreover, resonant X-ray interferometry would allow us to determine the positions of those prosthetic groups' metal ions within the profile structure with great precision.[34,35] Determining the monolayer's structure in such detail and measuring the rate of electron transfer to an underlying electrode would impose a very stringent test of electron transfer as both the distance *and* the medium through which transfer occurs would be known.

Conclusions

We have succeeded in producing LB monolayers of maquette peptides with the peptide helical axes oriented approximately normal to the plane of the solid support, even in cases when in the peptide is oriented parallel to the air/water interface in the precursor Langmuir monolayer. The experimentally obtained electron density profile structures agree qualitatively with projections computed from atomic coordinates obtained from model predictions or NMR measurements. The orientation of the molecules makes feasible the application of other techniques capable of studying the profile structures of these monolayers in greater detail, while the solid support could incorporate an electrode, permitting electrochemical studies of the function of the peptide with metalloporphyrin prosthetic groups bound. Variation between samples can be substantial and needs to be better controlled in the future to realize the potential of these monolayers as test systems for electron transfer theory.

Acknowledgment. The authors thank Dr. Francesc Rabanal for the model atomic coordinates of H10H24 and Dr. Brian Gibney for the atomic coordinates of the NMR solution structure of BB. This work was made possible through support from the NIH under Grants GM33525 and GM41048 and from the MRSEC Program of the NSF under Award Number DMR96-32598.

Supporting Information Available: Figures showing the determination of the thickness of the H10H24 film from the Patterson function (S1), $\Delta\rho_{exp}(z)$ and the model $\rho(z)$ functions constructed to agree with three H10H24 samples (S2 and S3), the thickness of a pure BBC16 film and a 4:1 PA/BBC16 film from the Patterson function (S4), and model $\rho(z)$ functions constructed for the BBC16-containing samples (S5). This material is available free of charge via the Internet at http://pubs.acs.org.

LA0009285

(33) Pilloud, D. L.; Rabanal, F.; Moser, C. C.; Dutton, P. L. *Biophys. J.* **1998**, *74*, A250.

(34) Blasie, J. K.; Stamatoff, J. *Annu. Rev. Biophys. Bioeng.* **1981**, *10*, 451−458.

(35) Pachence, J. M.; Fischetti, R. F.; Blasie, J. K.; *Biophys. J.* **1989**, *56*, 327−337.